International Journal of Biological Macromolecules 133 (2019) 428–435

Contents lists available at ScienceDirect

International Journal of Biological Macromolecules

journal homepage: http://www.elsevier.com/locate/ijbiomac

Correct partner makes the difference: Septin G-interface plays a critical role in amyloid formation

Patricia S. Kumagai [a,1], Carla S. Martins [a,1,2], Elisa M. Sales [b,c], Higor V.D. Rosa [a], Deborah C. Mendonça [a], Júlio Cesar P. Damalio [d], Francesco Spinozzi [e], Rosangela Itri [c], Ana Paula U. Araujo [a,*]

[a] Instituto de Física de São Carlos, Universidade de São Paulo, Av. João Dagnone, 1100, São Carlos, SP CEP 13563-120, Brazil
[b] IPT-Institute for Technological Research, Av. Prof. Almeida Prado, 532, São Paulo, SP CEP 05508-280, Brazil
[c] Instituto de Física, Universidade de São Paulo, Rua do Matão, 1371, São Paulo, SP CEP 05508-090, Brazil
[d] Instituto Federal de Educação e Tecnologia de São Paulo, Campus Avaré, Av. Prof. Celso Ferreira da Silva, 1333, Avaré, SP CEP 18707-150, Brazil
[e] Department of Life and Environmental Science, Polytechnic University of Marche, Via Brecce Bianche, 60131 Ancona, Italy

ARTICLE INFO

Article history:
Received 20 February 2019
Received in revised form 12 April 2019
Accepted 15 April 2019
Available online 16 April 2019

Keywords:
Septin
Heterocomplex
Amyloid

ABSTRACT

Septins are members of a group of GTP-binding proteins highly conserved in eukaryotes, being linked to diverse cell processes, such as cytokinesis and membrane association. On the other hand, the malfunction of septins is linked to several pathological processes including neurodegeneration and oncogenesis. Septins interact with each other forming heterocomplexes that polymerize in filaments. Two types of interface between septins alternate along the filament: the G-interface (involving the GTP binding sites), and the NC-interface. This work focuses on the physiological G-interface of SEPT2, used in the SEPT6G-SEPT2G heterodimer assembly, to verify the impact of this interaction on the thermostability and amyloid formation. We found that the SEPT6G-SEPT2G moves to an irreversible state with the ability to bind thioflavin-T at high temperatures, suggesting its amyloid-like nature. Noteworthy, this takes place at a higher temperature than the one observed to the single septins, showing greater thermal/structural stability. Taken together, our results show that in the absence of the partners, the septin becomes unstable and susceptible to amyloid aggregation/formation even in physiological temperatures, and the G-interface appears to have a critical role in this process.

1. Introduction

Septins are guanine nucleotide binding proteins recognized as an important component of the cytoskeletal system in several eukaryotic species [1–3]. They are present in a variety of organisms, such as fungi, animals and protists, but no septin gene has been reported in higher plants so far [4,5]. The number of codifying genes for septins is quite variable in each organism [6], it can be a single gene, as in the *Chlamydomonas reinhardtii* [4,7], two genes, as in *Caenorhabditis elegans* [8], or thirteen genes in *Homo sapiens* [9].

Structurally, septins consist of three conserved domains: a central GTP-binding domain (G-domain), and N- and C-domains of variable length. A peculiar characteristic of septins is their ability to form complexes and filaments in a particular order and symmetry, resulting in a nonpolar filament. According to sequence similarity, the human septins are classified in four different subgroups. Usually, a complex is formed by one septin of each subgroup, and they are interchangeable within the subgroup. They can form highly ordered structures, such as bundles and rings, which are the functional forms of septins [10–13].

To date, there are 20 three-dimensional structures of septins from diverse organisms deposited at the Protein Data Bank (https://www.rcsb.org). Among them, only one crystal structure is related to septin complex (PDB ID 2QAG, [14]), which forms septin filaments by repeating dimers of trimer units of septins 2-6-7 in a palindromic way. The septin subunits are assembled into filaments by the G-domain using conserved G- and NC-interfaces intercalated in the crystal, where the G-interface is stabilized by guanine nucleotides [14]. Septin 2-6-7 complex interfaces are considered as native/physiologic ones, but many non-physiological (promiscuous) interfaces have also been observed with single septins. For instance, Sirajuddin et al. [14] have demonstrated that the G-domain of human septin-2 (SEPT2G) forms a promiscuous homodimer in solution by the G-interface, having the NC- as its physiological interface in the heterocomplex.

Due to their plasticity, septins are ubiquitous protein and, consequently, are involved in diverse cellular functions, as cell division,

* Corresponding author at: Universidade de São Paulo, Instituto de Física de São Carlos, Departamento de Física e Ciências Interdisciplinares, Av. João Dagnone, 1100, Jd Santa Angelina, São Carlos, São Paulo CEP 13563-120, Brazil.
E-mail address: anapaula@ifsc.usp.br (A.P.U. Araujo).
[1] PS Kumagai and CS Martins contributed equally to this work.
[2] Present address: Institut Fresnel, Marseille, France.

https://doi.org/10.1016/j.ijbiomac.2019.04.105
0141-8130/

differentiation, apoptosis, etc.. Together with actin, microtubules and intermediate filaments, septins play an important role in cytoskeleton organization and cytokinesis [3]. Modifications, changes and/or alterations of these proteins, as overexpression or mutations, have been associated with some cancers, as well as spermatogenesis and schizophrenia [15–18]. Additionally, the human septin proteins, SEPT1, SEPT2 and SEPT4 were found in the brain plaques and tangles, being associated with Alzheimer's disease [19] and neurodegeneration.

Several experimental evidences have shown that protein aggregation can be triggered by mild changes in the environmental conditions, being that the proteins ability to aggregate is correlated with the decreased stability [20–22]. Strikingly, SEPT4 and SEPT2 were described forming amyloid-like filaments in vitro [23,24], suggesting that some septins could directly contribute to the protein aggregates observed in the brain of Alzheimer's disease patients. Additionally, SEPT3 was also demonstrated to form amyloid like structures in vitro [25]. It should be noted that, in all in vitro experiments, just a single septin was present and none straight connection with physiological septin filaments could be established.

In this scenario, it is tempting to suppose that the presence of a septin partner may be a determining factor for the correct interaction and, in a complementary way, that its absence could lead to the formation of the promiscuous and unstable interfaces of interaction. Moreover, it is not clear how this assumption is related to amyloid aggregation.

In an attempt to clarify these issues, we investigate the SEPT6G-SEPT2G heterodimer assembled by a physiological G-interface, aiming to verify the influence of this interaction on the thermal stability and the propensity of amyloid formation, in contrast with single septins. Our results indicate that the proper septin interaction at G-interface is an important factor to stabilize the heterodimer under physiological temperatures.

2. Materials and methods

2.1. Materials

The bacterial expression vectors (pETDuet and pRSFDuet) and strains were purchased from Novagen and the Ni-NTA resin, from Qiagen. The p*lasmid DNA purification kit was* purchased from Promega. Restriction endonucleases, isopropyl-b-D-thiogalactopyranoside (IPTG), T4 DNA ligase and Taq Polymerase were obtained from Fermentas-Thermo Scientific. The antibiotics, protein standard markers and Thioflavin-T (ThT) were purchased from Sigma. All other chemicals were of analytical grade.

2.2. Cloning, protein expression and purification

The DNA encoding G-domains of SEPT2 (corresponding to residues 35-308, GenBank access number NM_001008491.1), and SEPT6 (corresponding to residues 40-305, GenBank access number NM_015129.5), were generated by standard PCR protocols, starting from clones described in Nakahira et al. [26]. The PCR products were subcloned into the pRSFDuet (*Nde*I and *Xho*I) and pETDuet (*Bam*HI and *Hind* III) expression vectors, to produce SEPT2G and SEPT6G domains, respectively. The cloning sites used for pETDuet allowed us to produce SEPT6G in fusion with His-tag at N-terminus. *E. coli* Rosetta (DE3) strain was used as host for expression of SEPT6G and also for the SEPT6G-SEPT2G complex.

For coexpression, a total of 20 mL of an overnight culture of *E. coli* Rosetta (DE3) harboring both plasmids were inoculated into 1 L of fresh LB medium containing kanamycin (30 $\mu g \cdot mL^{-1}$), ampicillin (50 $\mu g \cdot mL^{-1}$) and chloramphenicol (34 $\mu g \cdot mL^{-1}$). The culture was grown at 37 °C, under shaking, until to mid log phase ($O.D._{600nm} = 0.6–0.8$). Subsequently, IPTG was added to a final concentration of 0.2 mM and the culture was incubated for 16 h at 18 °C. The cells were harvested by centrifugation and resuspended in 25 mM Tris-HCl pH 7.8, 500 mM NaCl, 5 mM $MgCl_2$, 5 mM β-mercaptoethanol and 5% v/v of glycerol, and disrupted by sonication. The suspension was then centrifuged at 6000*g* for 20 min at 4 °C, and the supernatant was loaded into a nickel affinity column (Ni-NTA, QIAGEN) pre-equilibrated with the same buffer used in lysis. The unbound proteins were eliminated by exhaustive washing, and SEPT6G-SEPT2G heterodimer was eluted by imidazole 400 mM added to the buffer. For SEPT6G, individually, the same protocol designed for the heterocomplex expression and purification was followed. The protein SEPT2G alone was produced as described in Damalio et al. [24].

Purified proteins eluted from affinity chromatography were then loaded into a HiLoad Superdex 200 16/600 GL column (GE Healthcare Life Sciences) pre-equilibrated with 25 mM Tris-HCl buffer, pH 7.8, containing 150 mM NaCl, 5 mM $MgCl_2$, 5 mM β-mercaptoethanol and 5% *v*/v of glycerol and driven by an Äkta purifier (GE Healthcare Life Sciences). For SEPT6G, the column used was Superdex 200 10/300 GL(GE Healthcare Life Sciences).

Protein concentration was determined based on its molar extinction coefficient [27] and, when necessary, the purified proteins were concentrated in an ultrafiltration system (Millipore) and/or submitted to buffer exchange, in order to reduce the additives and to allow the comparison with previous data for SEPT2G [24].

Polydispersity and oligomeric state of the pure protein samples were also monitored using SEC-MALS. Aliquot of 20 μL (2.0 $mg \cdot mL^{-1}$) of the SEPT6G-SEPT2G heterodimer was loaded into a WTC-030N5 molecular spinning column (Wyatt Technology) and analyzed by HPLC on a Waters 600 Controller following the protocol of the manufacturer. Coupled with chromatography, the DAWN TREOS miniature system (Wyatt Technology) determined mass distribution, size and composition, and the OptiLab T-REX system (Wyatt Technology) determined the differential refractive index. The data were processed using ASTRA7 software (Wyatt Technology).

2.3. Circular dichroism(CD) spectroscopy

The thermal unfolding of the recombinant proteins, SEPT6G–SEPT2G and SEPT6G, was monitored by far-UV CD spectroscopy, taking the spectra over a wavelength range from 280 to 195 nm, using 1 nm interval, with a number of 16 accumulations in a J-815 Jasco spectropolarimeter equipped with a temperature controller. CD spectra were measured from samples in a 0.1 cm quartz cuvettes. The protein concentration, in both cases, was approximately 3 μM in 25 mM Tris-HCl buffer, pH 7.8, containing 10% *v*/v of glycerol. Thermal denaturation measurements were performed by incubating the samples for 30 min at each temperature, up to 70 °C. All final CD spectra were processed with the CDTool software [28]. Processing consisted in averaging the individual scans, subtracting the respective baseline spectrum (containing the solution with all additives, except the protein), zeroing spectrum at 263–270 nm region, noise smoothing with Savitzky-Golay filter, and final data expressed in degree ellipticity scale.

2.4. Differential scanning calorimetry (DSC)

Calorimetric measurements were performed in a MicroCal VP-DSC instrument (Northampton, USA). The protein concentration was subsequently adjusted to 0.1–1.0 $mg \cdot mL^{-1}$ in 25 mM Tris-HCl buffer, pH 7.8, containing 10% v/v of glycerol. The thermal denaturation was performed from 20 to 80 °C with a heating rate of 60 °C/h. A buffer-buffer reference scan was made using the same conditions. The baseline subtraction, concentration normalization and data analyses were done by using the ORIGIN 7.0 software supplied by the manufacturer.

2.5. SAXS data collection and analyses

Septin G-domain SEPT2G (0.5 $mg \cdot mL^{-1}$), SEPT6G (0.4 $mg \cdot mL^{-1}$) and SEPT6G-SEPT2G (0.4 $mg \cdot mL^{-1}$) heterodimer were prepared in the

buffer 25 mM Tris-HCl, pH 7.8, 10% v/v glycerol as fresh as possible, and were kept into an ice container until transferred to the sample holder, in order to avoid precipitation/aggregation's effect. The temperature was controlled by a water circulating bath. The protein solution was equilibrated at the desired temperature for approximately 10 min before data acquisition. Time evolution of each sample was investigated at increasing temperature from 15 to 65 °C for SEPT6G-SEPT2G, and from 15 to 45 °C for SEPT2G and SEPT6G.

Small Angle X-ray Scattering (SAXS) data were acquired in the SAXS beamline at Brazilian Synchrotron Light Source, LNLS (Laboratório Nacional de Luz Síncrotron – Campinas/SP) with a sample to detector distance of 1.61 m, which results in a range of scattering vector modulus q from 0.005 to 0.25 Å^{-1}, where $q = (4\pi/\lambda)\sin\theta$, λ being the X-ray wavelength and 2θ the scattering angle.

Data were analyzed assuming that SAXS curves can be represented by the linear combination of the SAXS signals of different protein species in solution: dimers, cylinder-like aggregates representing septin oligomers and large aggregates whose scattering is given by the Porod's law asymptotic behavior proportional to q^{-4}. The scattering of septin dimers was calculated on the basis of the SEPT2G crystallographic homodimer structure (PDB ID 2QA5), since the molecular masses of septins studied in this work are similar. For further details, the reader is referred to Supplementary Information (SI). Model fittings to the experimental scattering were done by means of GENFIT software [29].

2.6. Thioflavin-T fluorescence assay

In order to detect amyloid-like filaments, Thioflavin-T (ThT) measurements were performed as previously described [24]. Briefly, SEPT6G–SEPT2G and SEPT6G at 5 μM in buffer solution (25 mM Tris-HCl, pH 7.8, 10% v/v glycerol) were incubated with 50 μM of ThT. Samples were excited at 450 nm and the emission at 482 nm was measured for a period of 90 min, in a K2 ISS Spectrofluorimeter. Measurements were held up to 60 °C. All intensity spectra were normalized to values between 0 and 1, after subtraction of the light scattering of the buffer. Data points were analyzed with the software Origin 7.5.

3. Results and discussion

3.1. Septin G-domains purification profile

The size exclusion chromatography (SEC) profile of the heterocomplex SEPT6G-SEPT2G presented two different peaks, showing the coexistence of monomers and dimers in solution, corresponding to the heterodimer and the excess of SEPT6G monomer (Fig. 1A). On the other hand, SEC purification of SEPT2G and SEPT6G displayed only one peak each, eluted in distinct volumes, indicating that they are in a dimeric and monomeric conformation, respectively (Fig. 1A). The size exclusion chromatography coupled with multi-angle light scattering (SEC-MALS) was also performed to monitor the oligomerization, homogeneity and quality of the samples. As can be seen from Fig. 1B, the SEC-MALS profile of SEPT6G-SEPT2G, obtained from the first peak of previous SEC step (Fig. 1A), exhibited a single monodisperse peak related to a molecular mass of 63 ± 1 kDa, consistent with heterodimers.

For fresh purified SEPT6G, SEC-MALS profile confirmed its monomeric conformation with molecular mass of 34 ± 1 kDa (Fig. S1). To monitor the stability of this sample, SEC-MALS measurements were made after following few hours of the samples sited on ice (Fig. S1). An increase in the peak corresponding to higher molecular mass and a decrease of the peak corresponding to the monomer were detected. This behavior probably is due to the formation of dimers and/or aggregates over time, reflecting the instability of the SEPT6G. Therefore, SEPT6G revealed to be a very unstable monomeric protein. Regarding SEPT2G, a previous study showed a homodimer with an apparent molecular mass of approximately 60 kDa in the same conditions [24].

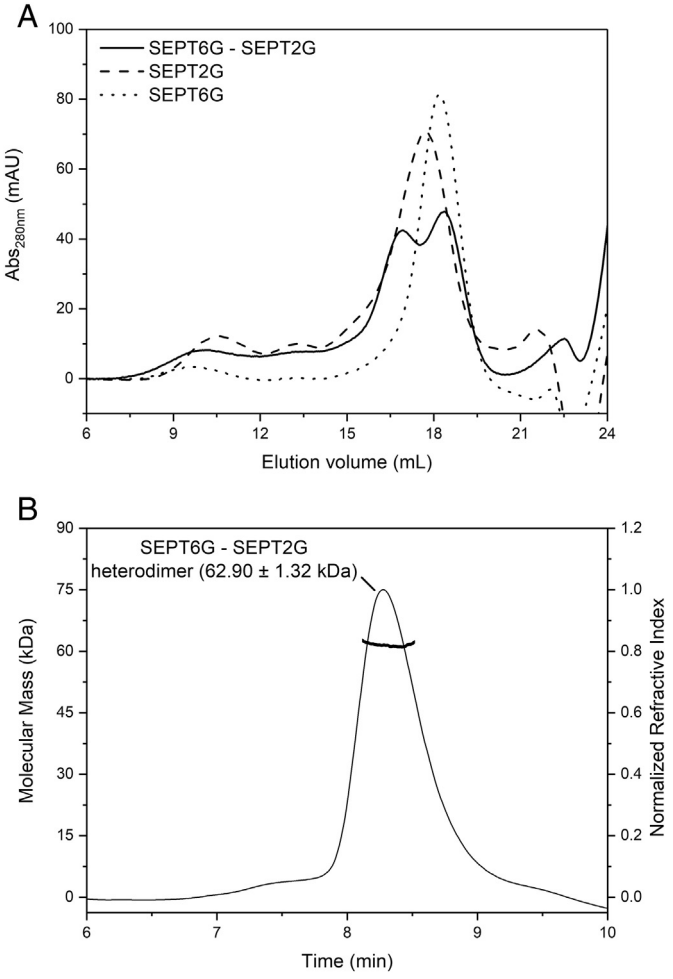

Fig. 1. Septin G-domains purification profile. (A) SEC profile of SEPT2G, SEPT6G and SEPT6G–SEPT2G. The SEPT2G was eluted as a dimer in solution, while the SEPT6G was eluted as a monomer. Meanwhile, the co-expression of SEPT6G–SEPT2G was eluted in two non-completely solved peaks, corresponding to the heterodimer and the excess of SEPT6G purified from the affinity chromatography. (B) SEC-MALS profile of SEPT6G–SEPT2G, following the previous SEC step. The variation of the differential refractive index showed a monodisperse sample, and the estimated molecular mass for the heterodimer amounted to 62.90 kDa.

3.2. Thermal and structural stability

Thermal and structural stability of the proteins were firstly monitored by CD spectroscopy (Fig. 2). As expected from the septin structures [14,24], the CD spectrum of the heterodimer SEPT6G–SEPT2G is characteristic of an α-helical containing protein (Fig. 2A), with two negative minima at 208 and 222 nm and one positive maximum at 198 nm. Note that the native conformation of SEPT6G-SEPT2G is structurally very stable until the temperature of 55 °C, i.e., all spectra look alike in terms of α-helical content. However, the temperature transition occurred between 55 and 60 °C, in which the CD spectrum acquires some β-sheet structure characteristics, with a minimum around 215 nm. Fig. 2B shows the thermal stability of SEPT6G, where the α-helical to β-sheet structure shift takes place between 25 and 37 °C, similarly to what has been previously observed for SEPT2G [12]. The percentages of secondary structure content for both proteins in different temperatures were estimated by DichroWeb server [30,31], and summarized in Table S1.

Due to the great stability of heterodimer observed in CD analyses, we have performed differential scanning calorimetry (DSC), with the aim of obtaining thermodynamic parameters of the septin G-domains thermal

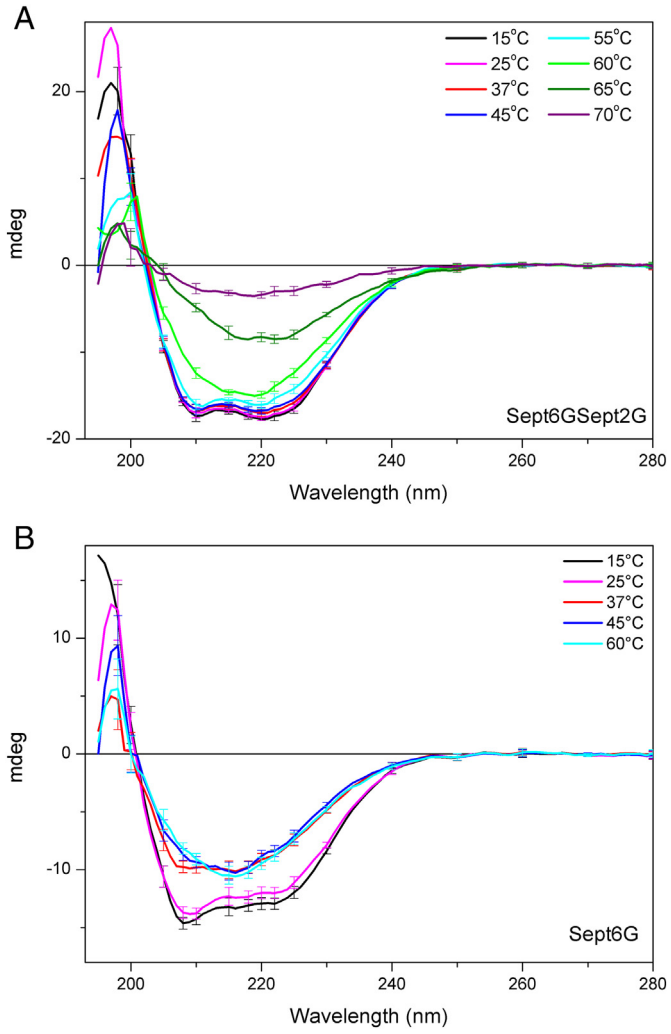

Fig. 2. CD spectra at increasing temperatures. (A) SEPT6G-SEPT2G: no significant change on the CD spectra is observed from 15 to 55 °C. Above this temperature a loss in the minima at 208 and 222 nm, characteristics of α-helix, can be observed in the spectral profile. (B) SEPT6G: the loss of the α-helix profile at 37 °C. Error bars represent the standard deviation of each measurement.

denaturation process. The thermograms of SEPT6G and SEPT6G-SEPT2G (reported in Fig. S2) show temperature transition (T_m) of 43 and 67 °C, respectively (Table 1). Furthermore, the greater values of enthalpy (ΔH_{cal}) and entropy (ΔS_{cal}) of the SEPT6G-SEPT2G compared to the SEPT6G, revealed a larger amount of energy is required to dismount the intramolecular interactions of the heterodimer (Table 1). Which means that the native contacts of heterodimer reflect the stronger nature of the physiologic G-interface. The transition temperatures obtained by DSC were slightly higher than the ones obtained by CD, this is due to the different conditions necessary to each experiment, mainly the heating rate, the transition temperature for each technique are considered significant. Anyway, the variation of transition temperature ΔT_m ~ 20 °C observed between SEPT6G (or SEPT2G) compared to the heterodimer was about the same magnitude in both methods.

Table 1
Temperature transition (T_m), enthalpy (ΔH_{cal}) and entropy (ΔS_{cal}) from septin G-domain proteins during the unfolding process based on the DSC thermograms of Fig. S2.

	T_m (°C)	ΔH_{cal} (kcal·mol^{-1})	ΔS_{cal} (kcal·°C^{-1}·mol^{-1})
SEPT6G	42.8	78.3	1.83
SEPT6G-SEPT2G	67.3	184.1	2.74

The thermodynamic parameters (T_m, ΔH_{cal} and ΔS_{cal}) obtained from DSC thermograms are summarized in Table 1.

It is known that the presence and nature of nucleotides can bias the stability of interfaces in hetero-oligomeric septins, and it might be an important fact to the septin pairing and assembly in physiologic conditions [32]. Therefore, we cannot discard that the lack of nucleotide retained can be one of the reasons for the SEPT6G instability and the greater stability of SEPT6G-SEPT2G as well. On the other hand, the promiscuous homodimers of SEPT2G, formed via the G-interface present bound nucleotide [32] and, even in this case, they also behave as SEPT6G, being unstable under physiological temperatures [19]. In this context, we decided not to consider nucleotide presence/absence in the other experiments.

In order to have a better insight about the thermo-stability of the SEPT6G-SEPT2G heterodimer in respect to its counter-partner SEPT2G and SEPT6G, SAXS experiments were then performed. The whole data set was analyzed by considering the possibility of having small aggregates (dimers), intermediate oligomers (cylinder-like aggregates) and undefined large aggregates coexisting in solution, being the percentage of each population a free fitting parameter (Eq. (1) SI).

Fig. 3 presents the results from *in-solution* SEPT6G-SEPT2G and Table 2 the percentage of each scattering species retrieved from the fitting to the experimental data. A perusal of the SAXS data evidences that all scattering curves overlap for temperature increasing from 15 to 45 °C, with no change up to 760 s of data acquisition. The upturn in I(q) at low q values is a fingerprint from the presence of high-order aggregates in solution. Interestingly, the model fitting (solid line) to the experimental data (open symbols, Fig. 3A) indeed reveals the coexistence of a large amount of SEPT6G-SEPT2G heterodimers (91%) with small amount of large aggregates (9%, Table 2). On the other hand, at 55 °C one can observe an evolution of the SEPT6G-SEPT2G co-assembly over time (Fig. 3B) where the percentage of dimers decreases from 85% in the beginning of the experiment to 66% after 760 s of measurement with the appearance of intermediate oligomers concomitantly with the increase in the percentage of large aggregates (Table 2). Of note, this temperature is in line with the secondary structural transition temperature observed by CD (Fig. 2A). Furthermore, for temperatures above 60 °C (Fig. 3C), the SAXS curves put in evidence the morphological transformation of heterodimers into large aggregates, since the percentage of heterodimers decreases abruptly from 66 to 20% from 55 to 65 °C (Table 2, 760 s) whereas the percentage of large aggregates raises from 17 to 70%. The number of small oligomers in equilibrium with dimers and large aggregates does not change significantly (Table 2). The parameters related to small SETP6G-SEPT2G oligomers represented by cylindrical scattering objects (Eq. (2) SI) are: radius $R = 72 \pm 8$ Å; length $L = 232 \pm 16$ Å and electron density contrast $\Delta\rho = 0.40 \pm 0.01$ e/Å^3.

In consonance with CD spectra, the large aggregates observed might be long amyloid-like fibers, due to identified α-helix to β-sheet shift at this temperature interval (Fig. 2). Additionally, ThT results described ahead also give support to such statement.

In order to compare the SEPT6G-SEPT2G heterodimer stability with that observed for the SEPT6G, Fig. 4 presents the corresponding SAXS curves with data acquisition up to 760 s. Strikingly at 13 °C (Fig. 4A), the presence of monomers was detected in small quantity (~3%), reflecting the instability of the monomer. However, the dimers conformations are predominant, approximately 96% (Table 3) with a tiny contribution of large aggregates. As it was shown by SEC/SEC-MALS analyses (Fig. S1), it is not expected the dimer conformation in the buffer solution used here. Probably, the dimers detected by SAXS coexist with small aggregates, and it is relating with low concentration or none of salt that provides formation of nonfunctional dimers and/or small aggregates.

In the temperatures of 25 and 37 °C (Fig. 4B and C, respectively), the analysis of SAXS data reveals the co-existence of dimers, intermediate cylindrical and large aggregates (Table 3). The percentage of monomers

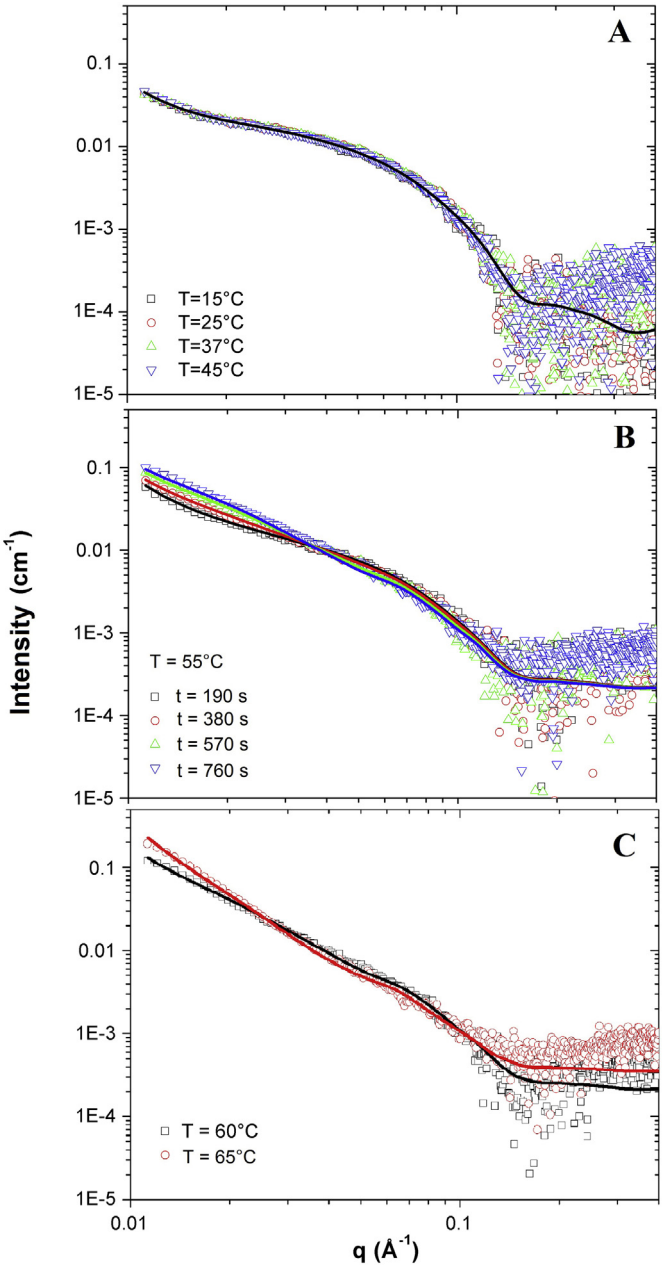

Fig. 3. SAXS data from SEPT6G-SEPT2G at increasing temperatures. (A) 15 to 45 °C: the SAXS curves do not change up to the measured acquisition time of 760 s; (B) 55 °C: SAXS data evolve from time acquisition $t = 190$ s to $t = 760$ s; (C) 60 and 65 °C: SAXS data at 190 s, where large aggregates are dominant in solution (see text for details).

Table 2
Percentage of dimers, cylinder-like and large aggregates (represented by Porod's law asymptotic behavior) for SEPT6G-SEPT2G obtained from model fittings (eqs. 1–3 SI) to the experimental SAXS data. The numbers in parenthesis indicate the uncertainty in each fitting parameter.

T (°C)	t (s)	$\%_{dimer}$	$\%_{cylinder}$	$\%_{Porod}$
15 to 45	760	91.0 (5)	–	9.0 (5)
55	190	85 (1)	4.1 (5)	10.9 (5)
	380	79 (1)	8 (1)	13 (1)
	570	71 (2)	12 (1)	17 (2)
60	760	66 (2)	17 (2)	17 (2)
	190	59 (2)	16 (2)	25 (2)
65	190	29 (1)	6 (1)	65 (1)
	380	27 (2)	8 (1)	65 (1)
	570	21 (1)	9 (1)	70 (1)
	760	20 (1)	10 (1)	70 (1)

in these conditions is insignificant, lesser than 0.1%, thus the monomer model was removed from these analyses. At 25 °C (Fig. 4B), SEPT6G showed a stable conformation over time, just a small variation in percentage of dimers and Porod's aggregates are observed (around 60 and 40%, respectively, on Table 3). Raising the temperature to 37 °C (Fig. 4C), it is possible to perceive the diminishing of dimers content and an increasing of cylindrical and Porod's aggregates over time. Further, the dimension of SEPT6G cylinder-like homo-oligomers resembles that found for SEPT6G-SEPT2G oligomer: radius $R = 75 \pm 2$ Å; length $L = 237 \pm 20$ Å and electron density contrast $\Delta\rho = 0.40 \pm 0.02$ e/Å^3.

Strikingly, the SAXS curves present significantly modified profiles upon temperature increase (45 °C on Fig. 4D). In this case, our modeling failed to reproduce the scattering data in the full measured q range. For this reason, the fitting data are not displayed in Table 3. This behavior might be related to the presence of undefined large aggregates (probably amorphous), not considered in our SAXS data analysis.

Therefore, it is clear from SAXS data that the SEPT6G homodimer is less resilient to oligomeric state transition upon temperature increase than the SEPT6G-SEPT2G heterodimer. Note that α-helical to β-sheet structure change was identified by CD for SEPT6G samples at temperature of 37 °C, and between 50 and 60 °C for SEPT6G-SEPT2G assembling. The thermal instability of SEPT6G aggregates must be related to the nonfunctional dimerization and, consequently, to its homo-oligomerization.

Thermal stability of SEPT2 observed by SAXS (up to 900 s of acquisition time) is similar to that here shown from SEPT6G self-assembling. The results are presented in Fig. S3 and Tables S2 and S3.

3.3. Amyloid formation

In order to evaluate the formation of higher order aggregates in solution, distinguishing amorphous aggregates from amyloid-like structures, Thioflavin-T (ThT) fluorescence assays were performed. Thioflavin-T is a well-known probe to amyloid fibrils, which has the fluorescence intensity increased just when binding to amyloid fibrils [33,34]. The ThT fluorescence (Fig. 5) was monitored at 482 nm, during 5400 s, in the same temperatures as CD and SAXS experiments.

For SEPT6G-SEPT2G (Fig. 5A), no fluorescence was detected in the temperature range of 25 to 45 °C, reflecting the greater stability of the physiological heterodimer. The intensity of ThT emission started to increase at 55 °C, indicating the formation of structure rich in β-sheet, which is strongly suggestive of amyloid formation. At 60 °C, it can rapidly form filaments (after 500 s), revealed by the abrupt increase of the fluorescence intensity followed by a little decrease of the same. The decline of ThT fluorescence is associated with the arrangement of other conformations, as large amorphous aggregates rather than amyloids, and subsequently precipitation. The morphology of the SEPT6G-SEPT2G amyloids was checked via negative staining TEM (Fig. S4), with a protein sample incubated 5 min at 65 °C. As we can see in the images, the morphology found is similar to large protofibrillar amyloid intermediates together with amorphous aggregates, as described in Malmos et al. [35].

ThT assay of SEPT6G is shown in Fig. 5B. At low temperatures, as 15 and 25 °C, no fluorescence was detected, and the intensity of ThT fluorescence emission started to increase at physiological temperature and above, reaching a constant emission. SEPT6G showed a prompt increase in the first few minutes at 45 °C, reflected in the sharp inclination of the emission curve. Overall, SEPT6G behaves most like SEPT2G [12] concerning to amyloid formation. Although, SEPT2G starts the formation of amyloid structures at 30 °C and reaches the maximum ThT emission at 45 °C, the pattern at higher temperatures, as 65 °C, is kept as constant emission.

4. Conclusion

After more than ten years of determination of the septin heterocomplex crystal structure [14], little is known concerning the

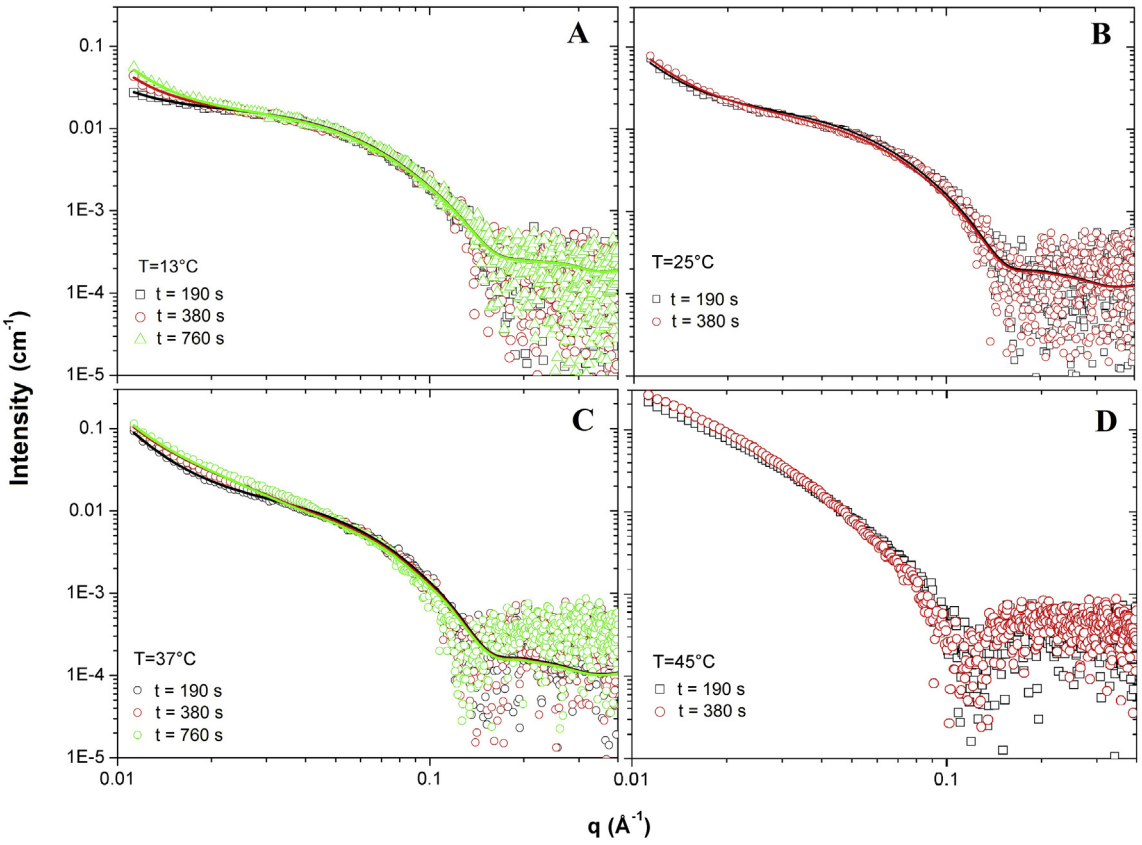

Fig. 4. Time evolution of SAXS data from SEPT6G in different temperatures. (A) 13 °C (B) 25 °C (C) 37 °C and (D) 45 °C.

architecture of its filament formation, the interface of interaction between septin subunits or even the characteristics of these interactions. On the other hand, some knowledge has been acquired in the past decade from the structure of several single septins solved. Here, we shed light to the physiological G-interface of septin complex and its relevance to the amyloid formation. Specifically, we investigated the G-interface of SEPT6G-SEPT2G complex, which is assembled as a heterodimer.

CD spectroscopy and SAXS experiments demonstrated the low thermal stability of SEPT2G and SEPT6G, and showed the structural transition temperature at physiological one. Afterward, ThT fluorescence revealed the amyloid nature of large aggregates evidenced by SAXS. SEPT6G results demonstrated that the G-domain is sufficient for amyloid-like structure formation, as seen previously for others human septins as SEPT2G [24], SEPT3GC [23] and SEPT4G [25]. Additionally, SEPT6G-SEPT2G heterodimer can also form amyloid structures but requires a higher temperature, around 55 °C, which is an environmental condition not compatible with homeostasis.

Table 3
Percentage of dimers, cylinder-like and large aggregates (represented by Porod's law asymptotic behavior) for SEPT6G obtained from model fittings (Eq. (1)–(3) SI) to the experimental SAXS data. The numbers in parenthesis indicate the uncertainty in each fitting parameter.

T (°C)	t (s)	$\%_{monomer}$	$\%_{dimer}$	$\%_{cylinder}$	$\%_{Porod}$
13	190	2.8 (7)	96.4 (5)	–	0.8 (5)
	380	3 (1)	95 (1)	–	2 (1)
	760	1.5 (5)	95.6 (5)	–	2.9 (5)
25	190	–	66.5 (1)	0.9 (5)	32.6 (5)
	380	–	60 (1)	2 (1)	38 (1)
37	190	–	55.5 (4)	0.7 (3)	43.8 (3)
	380	–	51.0 (5)	4 (1)	45 (1)
	760	–	48.5 (5)	4.7 (2)	46.8 (5)

The formation of amyloid-like structures needs a convergence of the characteristic α-helical content of septins to β-strand-like elements, which are then organized in cross-β-sheets. This new structural arrangement involves structural changes to assume the new conformation and, as shown by DSC, the SEPT6G-SEPT2G enthalpy and entropy values compared to the SEPT6G imply that a larger amount of energy is required to that rearrangement for the heterodimer. Thus, we suggest that the greater stability of the biological heterodimer has an important role in preventing amyloid structures from being formed under physiological temperature conditions. This behavior contrasts with the promiscuous homodimers via G-interface (as occurs with SEPT2G) and with the absence of G-interface interaction (as shown in SEPT6G).

Bringing our results to a physiological context of septins, it has already been suggested by Kinoshita [19] that the excessive aggregation of septin monomers could contribute to the recruitment of proteins involved in neurodegeneration, as in the case of the association described with the tau protein. Therefore, changes in the expression levels of septins leading to the prevalence of one of the components of the complex could contribute to the development of amyloid aggregates, as suggested by Hall and Finger [36]. Indeed, a recent proteomic study has shown that the levels of SEPT2 and SEPT3 are increased while SEPT5 is decreased in specific brain regions of Alzheimer's disease patients [37], which could lead to a septin subunit unbalance, triggering amyloid aggregation.

Taken together, our results reinforce this hypothesis, since they show that in the absence of the partners (or in the prevalence of a single septin), the septin becomes unstable and susceptible to amyloid aggregation/formation, even at physiological temperatures. Moreover, the G-interface appears to have a critical role in this process, since the interaction between SEPT2G and SEPT6G using this interface is sufficient to prevent amyloid formation in native condition. The process in which the G-interface interaction stabilizes the protein appears to be very specific, since the formation of promiscuous SEPT2G homodimer using the

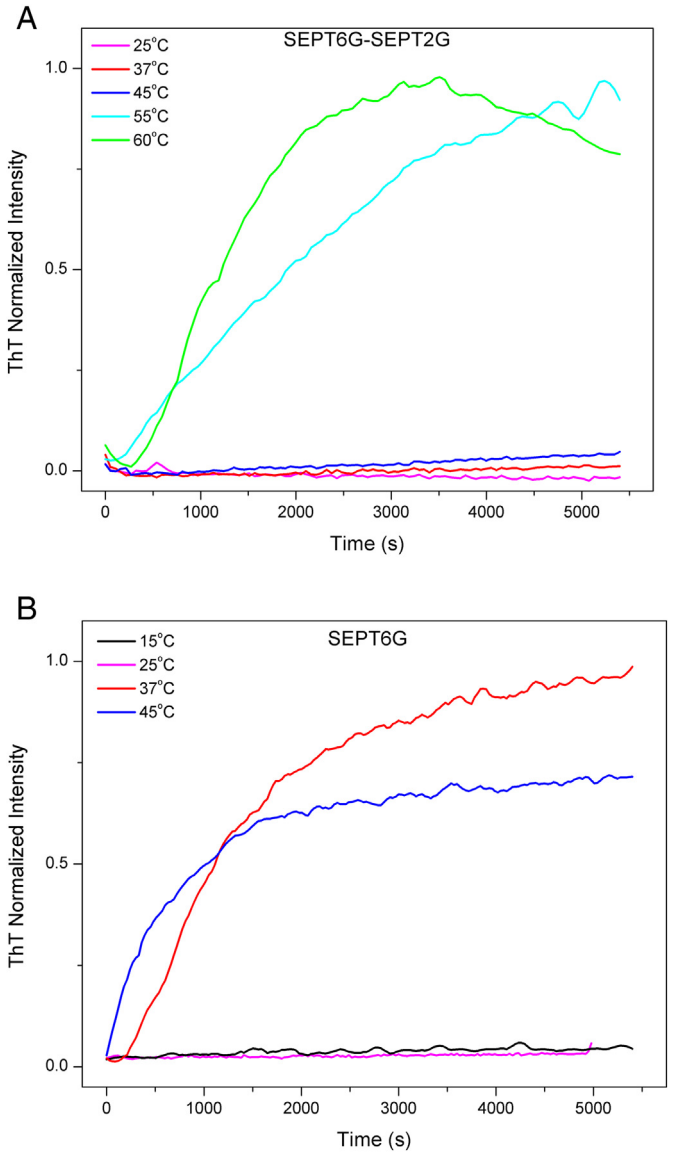

Fig. 5. ThT fluorescence assays as a function of temperature. (A) SEPT6G-SEPT2G: a very stable complex concerning to amyloid formation was observed. Almost non ThT emission was detected until 45 °C, an increase of intensity occurred at 55 °C, and at 60 °C, during the first 500 s, a rapid increase occurred followed by a little decline of emission, associated with the arrangement of other conformations. (B) SEPT6G: the maximum ThT fluorescence emission can be observed already at physiologic temperature, after circa *of* 1000 s.

same interface is not enough to stabilize the complex. Therefore, this mechanism provides a clear explanation of why single septins could lead to the formation of amyloids in physiological conditions.

Acknowledgments

The authors wish to acknowledge Dr. Ricardo De Marco and Dr. Richard C. Garratt, from University of São Paulo, for helpful discussions about septins. This research used resources of the Brazilian Synchrotron Light Laboratory (LNLS) and Brazilian Nanotechnology National Laboratory (LNNano), an open national facility operated by the Brazilian Center for Research in Energy and Materials (CNPEM) for the Brazilian Ministry for Science, Technology, Innovations and Communications (MCTIC). The SAXS1 beamline staff is acknowledged for the assistance during the experiments.

Funding

This work was supported by Sao Paulo Research Foundation (FAPESP) grant #2017/07709-6 to PSK, grant #2014/15546-1 to APUA and RI; Conselho Nacional de Desenvolvimento Cientifico e Tecnológico (CNPq) productivity fellowships to RI (#308295/2014-5) and APUA (#303229/2017-9).

Author contributions

CSM undertook of overexpression and purification of SEPT6G and SEPT6G-SEPT2G. PSK and CSM performed the CD and ThT fluorescence experiments. HVDR and PSK were responsible for DSC experiments. PSK, CSM and RI performed the SEPT6G and SEPT6G-SEPT2G SAXS measurements. JCPD, EMS and RI were responsible for production and data collection of SEPT2G SAXS experiments. EMS, FS and RI analyzed the SAXS data. DCM was responsible for TEM experiment. PSK, RI and APUA wrote the manuscript, with input from the other authors. APUA conceived and supervised the research study and secured the funding. All authors approved the final version of the manuscript.

Appendix A. Supplementary data

Supplementary data to this article can be found online at https://doi.org/10.1016/j.ijbiomac.2019.04.105.

References

[1] L.H. Hartwell, Genetic control of the cell division cycle in yeast. IV. Genes controlling bud emergence and cytokinesis, Exp. Cell Res. 69 (1971) 265–276.
[2] L. Cao, X. Ding, W. Yu, et al., Phylogenetic and evolutionary analysis of the septin protein family in metazoan, FEBS Lett. 581 (2007) 5526–5532.
[3] S. Mostowy, P. Cossart, Septins: the fourth component of the cytoskeleton, Nat. Rev. Mol. Cell Biol. 13 (2012) 183–194.
[4] R. Nishihama, M. Onishi, J.R. Pringle, New insights into the phylogenetic distribution and evolutionary origins of the septins, Biol. Chem. 392 (2011) 681–687.
[5] F. Pan, R.L. Malmberg, M. Momany, Analysis of septins across kingdoms reveals orthology and new motifs, BMC Evol. Biol. 7 (2007) 103.
[6] M. Kinoshita, The septins, Genome Biol. 4 (2003) 236.
[7] A.P.A. Pinto, H.M. Pereira, A.E. Zeraik, H. Ciol, F.M. Ferreira, J. Brandao-Neto, R. DeMarco, M.V.A.S. Navarro, C. Risi, V. Galkin, R.C. Garratt, A.P.U. Araujo, Filaments and fingers: novel structural aspects of the single septin from *Chlamydomonas reinhardtii*, J. Biol. Chem. 292 (2016) 10899–10911.
[8] C.M. John, R.K. Hite, C.S. Weirich, et al., The *Caenorhabditis elegans* septin complex is nonpolar, EMBO J. 26 (2007) 3296–3307.
[9] S.E. Russell, P.A. Hall, Septin genomics: a road less travelled, Biol. Chem. 392 (2011) 763–767.
[10] A.A. Bridges, H. Zhang, S.B. Mehta, P. Occhipinti, T. Tani, A.S. Gladfelter, Septin assemblies form by diffusion-driven annealing on membranes, Proc. Natl. Acad. Sci. U. S. A. 111 (2014) 2146–2151.
[11] G. Garcia III, G.C. Finnigan, L.R. Heasley, S.M. Sterling, A. Aggarwal, C.G. Pearson, E. Nogales, M.A. McMurray, J. Thorner, Assembly, molecular organization, and membrane-binding proper- ties of development-specific septins, J. Cell Biol. 212 (2016) 515–529.
[12] N.F. Valadares, H. d'Muniz Pereira, A.P.U. Araujo, R.C. Garratt, Septins structure and filament assembly, Biophys. Rev. 9 (2017) 481–500.
[13] K.A. Akhmetova, I.N. Chesnokov, S.A. Fedorova, Functional characterization of septin complexes, Mol. Biol. 52 (2018) 137–150.
[14] M. Sirajuddin, M. Farkasovsky, F. Hauer, D. Kuhlmann, I.G. Macara, M. Weyand, H. Stark, A. Wittinghofer, Structural insight into filament formation by mammalian septins, Nature 449 (2007) 311–317.
[15] D. Connolly, I. Abdesselam, P. Verdier-Pinard, et al., Septin roles in tumorigenesis, Biol. Chem. 392 (2011) 725–738.
[16] S. Mostowy, P. Cossart, Autophagyandthecyto- skeleton: new links revealed by intracellular pathogens, Autophagy 7 (2011) 780–782.
[17] E.A. Peterson, E.M. Petty, Conquering the complex world of human septins: implications for health and disease, Clin. Genet. 77 (2010) 511–524.
[18] P.A. Hall, S.E. Russell, The pathobiology of the septin gene family, J. Pathol. 204 (2004) 489–505.
[19] A. Kinoshita, M. Kinoshita, H. Akiyama, H. Tomimoto, I. Akiguchi, S. Kumar, M. Noda, J. Kimura, Identification of septins in neurofibrillary tangles in Alzheimer's disease, Am. J. Pathol. 153 (1998) 1551–1560.
[20] M.R. Hurle, L.R. Helms, L. Li, W. Chan, R. Wetzel, A role for destabilizing amino acid replacements in light-chain amyloidosis, Proc. Natl. Acad. Sci. U. S. A. 91 (1994) 5446–5450.
[21] M. Ramírez-Alvarado, J.S. Merkel, L. Regan, A systematic exploration of the influence of the protein stability on amyloid fibril formation *in vitro*, Proc. Natl. Acad. Sci. U. S. A. 97 (2000) 8979–8984.

[22] P. Alam, K. Siddiqi, S.K. Chturvedi, R.H. Khan, Protein aggregation: from background to inhibition strategies, Int. J. Biol. Macromol. 103 (2017) 208–219.
[23] W. Garcia, A.P.U. de Araujo, F. Lara, D. Foguel, M. Tanaka, T. Tanaka, R.C. Garratt, An intermediate structure in the thermal unfolding of the GTPase domain of human septin 4 (SEPT4/Bradeion-beta) forms amyloid-like filaments in vitro, Biochemistry 46 (2007) 11101–11109.
[24] J.C.P. Damalio, W. Garcia, J.N. Alves Macedo, I. De Almeida Marques, J.M. Andreu, R. Giraldo, R.C. Garratt, A.P.U. Araújo, Self assembly of human septin 2 into amyloid filaments, Biochimie 4 (2012) 628–636.
[25] M.G. Ortore, J.N.A. Macedo, A.P.U. Araujo, A. Ferrero, P. Mariane, F. Spinozzi, R. Itri, Structural and thermodynamic properties of septin 3 investigated by small-angle X-ray scattering, Biophys. J. 108 (2015) 2896–2902.
[26] M. Nakahira, J.N.A. Macedo, T.V. Seraphim, N. Cavalcante, T.A.C.B. Souza, J.C.P. Damalio, L.F. Reyes, E.M. Assmann, M.R. Alborghetti, R.C. Garratt, A.P.U. Araujo, N.I.T. Zanchin, J.A.R.G. Barbosa, J. Kobarg, A draft of human septin interactome, PLoS One 5 (2010), e13799.
[27] E. Gasteiger, et al., Protein identification and analysis tools on the ExPASy server, in: J.M. Walker (Ed.), The Proteomics Protocols Handook, Humana Press Inc, Totowa 2005, pp. 571–607.
[28] J.G. Lees, B.R. Smith, B.A. Wallace, CDtool - an integrated software package for circular dichroism spectroscopic data processing, analysis, and archiving, Anal. Biochem. 332 (2004) 285–289.
[29] F. Spinozzi, C. Ferrero, M.G. Ortore, A.D.M. Antolinos, P. Mariani, Genfit: software for the analysis of small-angle X-ray and neutron scattering data of macromolecules in solution, J. Appl. Crystallogr. 47 (2014) 1132–1139.
[30] L. Whitmore, B.A. Wallace, DICHROWEB, an online server for protein secondary structure analyses from circular dichroism spectroscopic data, Nucleic Acids Res. 32 (2004) W668–W673.
[31] L. Whitmore, B.A. Wallace, Protein secondary structure analyses from circular dichroism spectroscopy: methods and reference databases, Biopolymers 89 (2008) 392–400.
[32] M. Sirajuddin, M. Farkasovsky, E. Zent, A. Wittinghofer, GTP-induced conformational changes in septins and implications for function, Proc. Nat. Acad. Sic. USA 106 (2009) 16592–16597.
[33] H. Naiki, K. Higuchi, M. Hosokawa, T. Takeda, Fluorometric determination of amyloid fibrils in vitro using the fluorescent dye, thioflavin T1, Anal. Biochem. 177 (1989) 244–249.
[34] H. LeVine 3rd, Thioflavine T interaction with synthetic Alzheimer's disease beta-amyloid peptides: detection of amyloid aggregation in solution, Protein Sci. 2 (1993) 404–410.
[35] K.G. Malmos, et al., ThT 101: a primer on the use of thioflavin T to investigate amyloid formation, Amyloid 24 (2017) 1–16.
[36] P.A. Hall, F.P. Finger, Septins and human disease, in: A. Peter, S.E. Hall, H. Russell, J.R. Pringle (Eds.), The Septins, John Wiley & Sons, Ltd., West Sussex 2008, pp. 295–318.
[37] E. Tokhtaeva, J. Capri, E.A. Marcus, J.P. Whitelegge, V. Khuzakhmetova, E. Bukharaeva, et al., Septin dynamics are essential for exocytosis, J. Biol. Chem. 290 (2015) 5280–5297.